Geometric Graph Convolutional Neural Networks

Przemysław Spurek[1], **Tomasz Danel**[1], **Jacek Tabor**[1], **Marek Śmieja**[1],
Łukasz Struski[1], **Agnieszka Słowik**[2], **Łukasz Maziarka**[1]

[1]Faculty of Mathematics and Computer Science, Jagiellonian University
[2]Department of Computer Science and Technology, University of Cambridge
przemyslaw.spurek@uj.edu.pl

Abstract

Graph Convolutional Networks (GCNs) have recently become the primary choice for learning from graph-structured data, superseding hash fingerprints in representing chemical compounds. However, GCNs lack the ability to take into account the ordering of node neighbors, even when there is a geometric interpretation of the graph vertices that provides an order based on their spatial positions. To remedy this issue, we propose Geometric Graph Convolutional Network (geo-GCN) which uses spatial features to efficiently learn from graphs that can be naturally located in space. Our contribution is threefold: we propose a GCN-inspired architecture which (i) leverages node positions, (ii) is a proper generalisation of both GCNs and Convolutional Neural Networks (CNNs), (iii) benefits from augmentation which further improves the performance and assures invariance with respect to the desired properties. Empirically, geo-GCN outperforms state-of-the-art graph-based methods on image classification and chemical tasks.

Introduction

Convolutional Neural Networks (CNNs) outperform humans on visual learning tasks, such as image classification (Krizhevsky, Sutskever, and Hinton 2012), object detection (Seferbekov et al. 2018) or image captioning (Yang et al. 2017). They have also been successfully applied to text processing (Kim 2014) and time series analysis (Yang et al. 2015). Nevertheless, CNNs cannot be easily adapted to irregular entities, such as graphs, where data representation is not organised in a grid-like structure.

Graph Convolutional Networks (GCNs) attempt to mimic CNNs by operating on spatially close neighbors. Motivated by spectral graph theory, Kipf and Welling (Kipf and Welling 2016) use fixed weights determined by the adjacency matrix of a graph to aggregate labels of the neighbors. Velickovic et al. (Veličković et al. 2017) use attention mechanism to learn the strength of these weights. In most cases, the design of new GCNs is based on empirical intuition and there has been little investigation regarding their theoretical properties (Xu et al. 2018). In particular, there is no evident correspondence between classical CNNs and GCNs.

The code is available at https://github.com/gmum/geo-gcn.
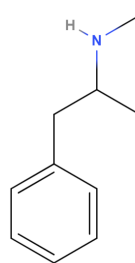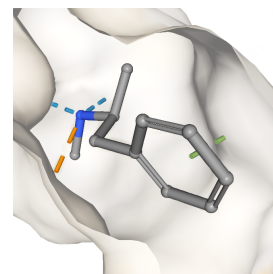
(a) Structural formula   (b) Example conformation

Figure 1: The graph representation of a compound (structural formula) is shown on the left. Vertices denote atoms, and undirected edges represent chemical bonds. On the right, the 3D view (conformation) of the same molecule is depicted along with its interactions with a target protein.

In many cases, graphs are coupled with a geometric structure. In medicinal chemistry, the three-dimensional structure of a chemical compound, called a molecular conformation, is essential in determining the activity of a drug towards a target protein (Figure 1). Similarly, in image processing tasks, pixels of an image are organised in a two dimensional grid, which constitutes their geometric interpretation. However, standard GCNs do not take spatial positions of the nodes into account, which is a considerable difference between GCNs and CNNs. Moreover, in the case of images, geometric features allow to augment data with translation or rotation and significantly enlarge a given dataset, which is crucial when the number of examples is limited.

In this paper, we propose Geometric Graph Convolutional Networks (geo-GCN), a variant of GCNs, which is a proper generalisation of CNNs to the case of graphs. In contrast to existing GCNs, geo-GCN uses spatial features of nodes to aggregate information from the neighbors. On one hand, this geometric interpretation is useful to model many real examples of graphs such as graphs of chemical compounds. In this case, we are able to perform data augmentation by rotating a given graph in a spatial domain and, in consequence, improve network generalisation when the amount of data is limited. On the other hand, a single layer of geo-GCN can be

parametrised so that it returns a result identical to a standard convolutional layer on grid-like objects, such as images (see Theorem 1).

The proposed method was evaluated on various datasets and compared with the state-of-the-art methods. We applied geo-GCN to classify images and incomplete images represented as graphs. We also tested the proposed method on chemical benchmark datasets. Experiments demonstrate that combining spatial information with data augmentation leads to more accurate predictions.

Our contributions can be summarised as follows:

- We show how to use geometric features (spatial coordinates) in GCNs.

- We prove that geo-GCN is a proper generalisation of GCNs and CNNs.

- In contrast to existing approaches, geo-GCN allows to perform graph augmentation, which further improves performance of the model.

Related work

The first instances of Graph Neural Networks were proposed in (Gori, Monfardini, and Scarselli 2005) and (Scarselli et al. 2008). These authors designed recursive neural networks which iteratively propagate node labels until reaching a stable fixed point. Recursive graph neural network were further developed by (Li et al. 2015) who used gated recurrent units for learning graph representation.

Recent approaches for graph processing rely on adapting convolutional neural networks to graph domain (graph convolutional network – GCNs). The first class of methods is based on spectral representation of graphs. The authors of (Bruna et al. 2013), (Henaff, Bruna, and LeCun 2015) and (Defferrard, Bresson, and Vandergheynst 2016) defined spectral filters which operate on the graph spectrum. Kipf and Welling (Kipf and Welling 2016) significantly simplified this process by restricting by restricting the neighborhood to only first-order neighbors. In this approach, convolutional layers followed by non-linear activity functions were stacked to process graph structure sequentially. This work was also extended to higher-order neighborhood (Zhou and Li 2017). In (Li et al. 2018), the notion of neighborhood in GCNs was generalized and a distance metric for graph was learned by spectral methods. The authors of (Wu et al. 2019) showed that removing nonlinearities from GCNs further reduces their complexity, but does not affect heavily the performance. Unfortunately, spectral methods are domain-dependent, which means that GCNs trained on one graph cannot be trivially transferred to another graph with a different spectral structure.

The second variant of GCNs does not use Laplacian basis to aggregate node neighbors but attempts to train convolutional filter for this purpose. To deal with varied-sized neighborhoods and to preserve the parameter sharing property of CNNs, (Duvenaud et al. 2015) used a specific weight matrix for each node degree. Subsequent work (Hamilton, Ying, and Leskovec 2017) used sampling strategy to extract a fixed size neighborhood. The authors of (Monti et al. 2017) used

spatial features to construct convolutional filters. In contrast to our approach, they transform geometric features using a predefined Gaussian kernels and do not focus on generalizing classical CNNs. In (Veličković et al. 2017), multi-head self attention was used to train individual weights for each pair of nodes. To account edge similarities, which appears natural in the chemical domain, the authors of (Shang et al. 2018) applied attention mechanism for edges. In (Gilmer et al. 2017) graph and distance information were integrated in a single model, which allowed to achieve strong performance on molecular property prediction benchmarks. Moreover, not only graph distances, but also three-dimensional atom coordinates are useful in molecular predictions as it was emphasized by (Cho, Choi, and others 2018) who introduced the 3DGCN architecture. They integrated matrix of relative atom positions into GCN architecture. However, 3DGCN is a chemistry-inspired model which does not aim to generalize CNNs.

While many variants of graph neural networks achieve impressive performance, their design is mostly based on empirical intuition and evaluation. The work of (Xu et al. 2018) investigates theoretical properties of neural networks operating on graphs. Based on graph isomorphism test, they formally analyze discriminative power of popular GNN variants (Kipf and Welling 2016), (Hamilton, Ying, and Leskovec 2017) and show that they cannot learn to distinguish certain simple graph structures. In a similar spirit, our geo-GCN is a theoretically justified generalization of classical CNNs to the case of graphs.

Geometric graph convolutions

In this section, we introduce geo-GCN. First, we recall a basic construction of standard GCNs. Next, we present the intuition behind our approach and formally introduce geo-GCN. Finally, we discuss practical advantages of geometric graph convolutions.

Let $G = (V, A)$ be a graph, where $V = \{v_1, \ldots, v_n\}$ denotes a set of nodes (vertices) and $A = [a_{ij}]_{i,j=1}^n$ represents edges. We put $a_{ij} = 1$ if v_i and v_j are connected by a directed edge and $a_{ij} = 0$ if the edge is missing. Each node v_i is represented by a d-dimensional feature vector $x_i \in \mathbb{R}^d$. Typically, graph convolutional neural networks transform these feature vectors over multiple subsequent layers to produce the final prediction.

Graph convolutions. Let $H = [h_1, \ldots, h_n]$ denote the matrix of node features being an input to a convolutional layer, where h_i are column vectors. The dimension of h_i is determined by the number of filters used in previous layer. Clearly, $X = [x_1, \ldots, x_n]$ is the input representation to the first layer.

A typical graph convolution is defined by combining two operations. For each node v_i, feature vectors of its neighbors $N_i = \{j : a_{ij} = 1\}$ are first aggregated:

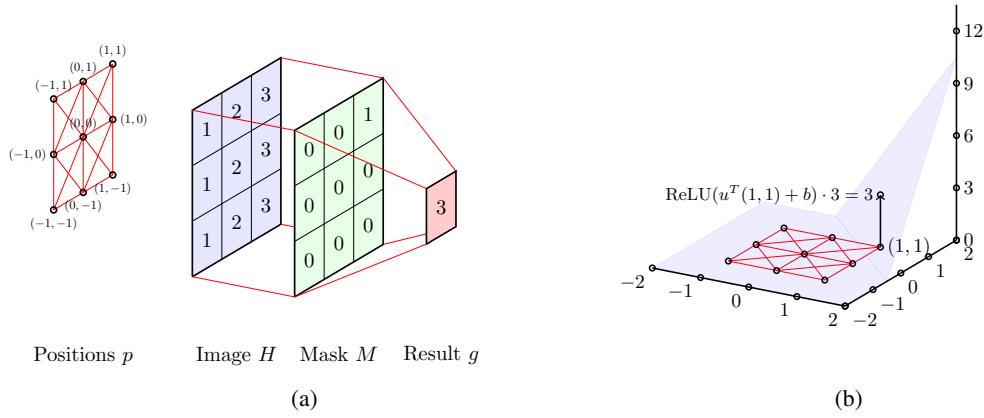$$\bar{h}_i = \sum_{j \in N_i} u_{ij} h_j. \tag{1}$$

Figure 2: Intuition behind our approach. On the left, the result of applying a convolutional filter M to the image H, which extracts the top-right neighbor. The positions grid p represents spatial coordinates of the pixels; the neighbors are connected with an edge. Analogous convolution can be applied to a geometric graph representation, as shown on the right: ReLU applied to the linear transformation of the spatial features of the image graph (with $u = (2,2)^T$ and $b = -3$) allows to select (and possibly modify) the top-right neighbor, see Example 1 for details.

The weights $u_{ij} \in \mathbb{R}$ are either trainable ((Veličković et al. 2017) applied attention mechanism) or determined by A ((Kipf and Welling 2016) motivated their selection using spectral graph theory).

Next, standard MLP is applied to transform the intermediate representation $\bar{H} = [\bar{h}_1 \ldots, \bar{h}_n]$ into the final output of a given layer:

$$\text{MLP}(\bar{H}; W) = \text{ReLU}(W^T \bar{H} + b), \qquad (2)$$

where a trainable weight matrix $W = [w_1, \ldots, w_n]$ is defined by column vectors w_i. The dimension of w_i determines the dimension of the output feature vectors.

Intuition behind geometric graph convolutions. Classical GCNs operate on the neighborhood given by the adjacency matrix. In some applications, nodes are additionally described by spatial coordinates. For example, the position of each pixel can be expressed as a pair of integers. Analogically, every conformation of chemical compound is a 3-dimensional geometrical graph, where each atom is located in the $\mathbb{R}^3$ space. The adjacency matrix is not able to preserve the whole information about the graph geometry. In particular, it is not possible to construct an analogue of classical convolution only from adjacency matrix and feature vectors. In our approach, we show how to include this spatial information in graph convolutions to construct a proper generalization of classical convolutions.

To proceed further, we need to introduce notation concerning convolutions (in the case of images). For simplicity we consider only convolutions without pooling. In general, given a mask $M = [m_{i'j'}]_{i',j' \in \{-k..k\}}$ its result on the image $H = [h_{ij}]_{i \in \{1..N\}, j \in \{1..K\}}$ is given by

$$M * H = G = [g_{ij}]_{i \in \{1..N\}, j \in \{1..K\}},$$

where

$$g_{ij} = \sum_{\substack{i'=-k..k:\, i+i' \in \{1..N\}, \\ j'=-k..k:\, j+j' \in \{1..K\}}} m_{i'j'} h_{i+i', j+j'}.$$

To present an intuition behind our approach, let us show how to mimic a classical linear convolution based on graph representation of the image.

Example 1. *For simplicity, let us consider a linear convolution given by the mask*

$$M = \begin{bmatrix} 0 & 0 & 1 \\ 0 & 0 & 0 \\ 0 & 0 & 0 \end{bmatrix}.$$

Observe that as the result of this convolution on the image H, every pixel is exchanged by its right upper neighbor, see Figure 2. Now we understand the image as a graph, where the neighborhood N_p of the pixel with coordinates $p = (p_x, p_y)^T$ is given by the pixels with coordinates $q = (q_x, q_y)^T$ such that $q - p \in \{-1, 0, 1\}^2$.

Given a vector $u \in \mathbb{R}^2$ and a bias $b \in \mathbb{R}$ we can define the (intermediate) graph operation by

$$g_p = \bar{h}_p(u, b) = \sum_{q \in N_p} \text{ReLU}(u^T(q - p) + b) h_q.$$

Consider now the case when $u = 2 \cdot \mathbb{1}, b = -3$, where $\mathbb{1} = (1,1)^T$. One can easily observe that

$$\text{ReLU}(u^T z - b) = \begin{cases} 0, & \text{for } z \neq \mathbb{1} \\ 1, & \text{for } z = \mathbb{1}, \end{cases}$$

where $z = q - p \in \{-1, 0, 1\}^2$.

Consequently, we obtain that $g_p = h_{p+\mathbb{1}}$, which equals the result of the considered linear convolution.
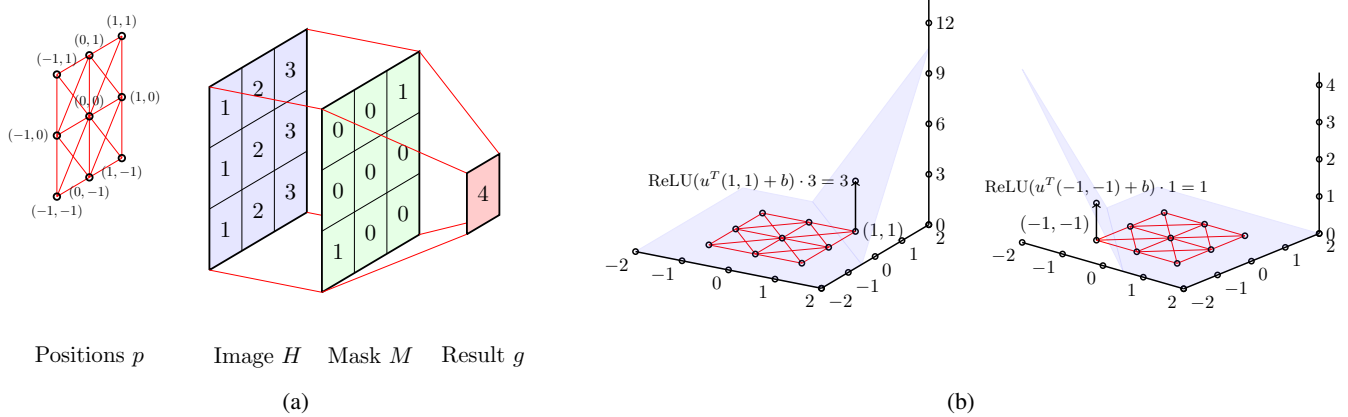
Positions p	Image H	Mask M	Result g		

(a)

(b)

Figure 3: Intuition behind our approach with more complex filter. The result of applying a convolutional filter M to the image H is presented on the left. This operation can be obtained from the image graph representation (on the right) by extracting two opposite corner values (with $u = (2,2)^T, b = -3$ and $u = (-2,-2)^T, b = -3$) and summing them, see Example 2 for details.

Example 2. *Now, let us consider the mask, see Figure 3:*

$$M = \begin{bmatrix} 0 & 0 & 1 \\ 0 & 0 & 0 \\ 1 & 0 & 0 \end{bmatrix}.$$

This convolution cannot be obtained from graph representation using a single transformation as in previous example.

To formulate this convolution, we define two intermediate operations for $k = 1, 2$:

$$\bar{h}_p(u_k, b_k) = \sum_{q \in N_p} \text{ReLU}(u_k(q - p) + b_k)h_q.$$

where $u_1 = 2 \cdot \mathbb{1}, b_1 = -3$ and $u_2 = -2 \cdot \mathbb{1}, b_2 = -3$. The first operation extracts the right upper corner, while the second one extracts the left bottom corner, i.e.

$$\bar{h}_p(u_1, b_1) = 1 \cdot h_{p+\mathbb{1}} \text{ and } \bar{h}_p(u_2, b_2) = 1 \cdot h_{p-\mathbb{1}}.$$

Finally, we put

$$\bar{h}_p = \begin{bmatrix} \bar{h}_p(u_1, b_1) \\ \bar{h}_p(u_2, b_2) \end{bmatrix} = \begin{bmatrix} h_{p+\mathbb{1}} \\ h_{p-\mathbb{1}} \end{bmatrix}.$$

Making an additional linear transformation (analogical to (2) with $w_p = (1,1)^T$), we obtain:

$$g_p = w_p^T \bar{h}_p = 1 \cdot h_{p+\mathbb{1}} + 1 \cdot h_{p-\mathbb{1}}.$$

As demonstrated in the above examples classical linear convolutions can be obtained from graphs by appropriate adaptation of (1) using spatial features. Based on this intuition, the precise formulation of geometric graph convolution is presented in the following paragraph. The complete proof that every linear convolution can be rewritten using geo-GCN is given in the next section.

Geometric graph convolutions. To formalize the above intuition, we define our geometric graph convolutions. We assume that each node v_i is additionally identified with its coordinates $p_i \in \mathbb{R}^t$. In contrast to standard features x_i,

we will not change p_i across layers, but only use them to construct better graph representation. For this purpose, we replace (1) by:

$$\bar{h}_i(u, b) = \sum_{j \in N_i} \text{ReLU}(u^T(p_j - p_i) + b)h_j, \qquad (3)$$

where $u \in \mathbb{R}^t, b \in \mathbb{R}$ are trainable. The pair u, b plays a role of a convolutional filter which operates on the neighborhood of v_i. The relative positions in the neighborhood are transformed using a linear operation combined with non-linear ReLU function. This scalar is used to weigh the feature vectors h_j in a neighborhood.

By the analogy with classical convolution, this transformation can be extended to multiple filters (as in Example 2). Let $U = [u_1, \ldots, u_k]$ and $b = [b_1, \ldots, b_k]$ define k-filters. The intermediate representation $\bar{h}_i$ is a vector defined by:

$$\bar{h}_i = \left[\bar{h}_i(u_1, b_1), \ldots, \bar{h}_i(u_k, b_k) \right].$$

Finally, we apply MLP transformation in the same manner as in (2) to transform these feature vectors.

Practical consequences. In practice, the number of training data is usually too small to provide sufficient generalization. To overcome this problem, one can perform data augmentation to produce more representative examples. In computer vision, data augmentation is straightforward and relies on rotating or translating the image. Nevertheless, in the case of classical graph structures, analogical procedure is difficult to apply. This is a serious problem in medicinal chemistry, where the goal is to predict biological activity based only on a small amount of verified compounds. The introduction of spatial features and our geometric graph convolutions allow us to perform data augmentation in a natural way, which is not possible using only the adjacency matrix.

The formula (3) is invariant to the translation of spatial features, but its value depends on rotation of graph. In consequence, the rotation of the geometrical graph leads to different values of (3). Since in most domains the rotation does not

affect the interpretation of object described by such graph (e.g. rotation does not change the chemical compound although one particular orientation may be useful when considering binding affinity, i.e. how well a given compound binds to the target protein), we can use this property to produce more instances of the same graph. This reasoning is exactly the same as in the classical view of image processing.

In addition, chemical compounds can be represented in many conformations. In a molecule, single bonds can rotate freely. Each molecule seeks to reach minimum energy, and thus some conformations are more probable to be found in nature than others. Because there are multiple stable conformations, augmentation helps to learn only meaningful spatial relations. In some tasks, conformations may be included in the dataset, e.g. in binding affinity prediction active conformations are those formed inside the binding pocket of a protein (see Figure 1b). Such a conformation can be discovered experimentally, e.g., through crystallization.

Theoretical Analysis

As shown above, introducing geometric features makes the processing of graphs similar to the way of image processing. In this part, we make this statement even more evident. Namely, we formally prove that our geometric graph convolutions generalise classical convolutions used in the case of images. In other words, we show that the appropriate parametrisation of geometric graph convolutions leads to the classical convolutions.

Theorem 1. *Let $M = [m_{i'j'}]_{i',j' \in \{-k..k\}}$ be a given convolutional mask, and let $n = (2k+1)^2$ (number of elements of M). Then there exist $u \in \mathbb{R}^2$, $b_1, \ldots, b_n \in \mathbb{R}$ and $w \in \mathbb{R}^n$ such that*

$$M * H = \sum_{i=1}^n w_i \bar{H}(u, b_i).$$

Proof. Let $P \subset \mathbb{R}^2$ denote all possible positions in the mask M, i.e. $P = \left\{ [i', j']^T : i', j' \in \{-k, \ldots, k\} \right\}$.

Let $u \in \mathbb{R}^2$ denote an arbitrary vector which is not orthogonal to any element from $P - P$. Then

$$u^T p \neq u^T q \text{ for } p, q \in P, p \neq q.$$

Consequently, we may order the elements of P so that $u^T p_1 > \ldots > u^T p_n$. Let M_i denote the convolutional mask, which has value one at the position p_i, and zero otherwise.

Now we can choose arbitrary b_i such that

$$b_i \in (-u^T p_i, -u^T p_{i+1}) \text{ for } i = 1..n-1, b_n > -u^T p_n,$$

for example one may take

$$b_i = -u^T \frac{p_i + p_{i+1}}{2} \text{ for } i < n, b_n = -u^T p_n + 1.$$

Then observe that

$\bar{H}(u, b_1) = (u^T p_1 + b_1) \cdot M_1 * H,$
$\bar{H}(u, b_2) = (u^T p_1 + b_2) \cdot M_1 + (u^T p_2 + b_2) \cdot M_2 * H,$

and generally for every $k = 1..n$ we get

$$\bar{H}(u, b_k) = \sum_{i=1}^k (u^T p_i + b_k) M_i * H,$$

where all the coefficients in the above sum are strictly positive.

Consequently,

$$M_1 * H = \frac{\bar{H}(u, b_1)}{u^T p_1 + b_1},$$

and we obtain recursively that

$$M_k * H = \frac{1}{u^T p_k + b_k} \bar{H}(u, b_k) - \frac{1}{u^T p_k + b_k} \sum_{i=1}^{k-1} (u^T p_i + b_k) M_i * H,$$

which trivially implies that every convolution $M_k * H$ can be obtained as a linear combination of $(\bar{H}(u, b_i))_{i=1..k}$.

Since an arbitrary convolution $M = [m_{ij}]$ is given by $M = \sum_{i=1}^n m_{p_i} M_i$, we obtain the assertion of the theorem. $\square$

On the other hand, if we put all spatial features p_i to 0, then (3) reduces to:

$$\bar{h}_i(u, b) = \sum_{j \in N_i} \text{ReLU}(b) h_j.$$

This gives a vanilla graph convolution, where the aggregation over neighbors does not contain parameters. We can also use different $b = u_{ij}$ for each pair of neighbors, which allows to mimic many types of graph convolutions.

Experiments

We verified our model on graphs with a natural geometric interpretation. We took into account graphs constructed from images as well as graphs of chemical compounds.

Image graph classification

In the first experiment, we consider the well-known MNIST dataset. We represent the images as graphs in two ways following (Monti et al. 2017). In the first case, each node corresponds to a pixel from the original image, making a regular grid with connections between adjacent pixels. The node has 2-dimensional location, and it is characterized by a 1-dimensional pixel intensity. In the second variant, nodes are constructed from an irregular grid consisting of 75 superpixels. In the latter case, the edges are determined by spatial relations between nodes using k-nearest neighbors.

We tune the hyperparameters of geo-GCN using a random search with a fixed budget of 100 trials, see supplementary material for details. We compare our method with the results reported in the literature by state-of-the-art methods used to process geometrical shapes: ChebNet (Defferrard, Bresson, and Vandergheynst 2016), MoNet (Monti et al. 2017), and SplineCNN (Fey et al. 2018).

The results presented in Table 1 show that geo-GCN outperforms comparable methods on both variants on MNIST dataset. Its performance is slightly better than SplineCNN, which reports state-of-the-art results on this task.

Table 1: Classification accuracy on two graph representations of MNIST.

Method	Grid	Superpixels
ChebNet	99.14%	75.62%
MoNet	99.19%	91.11%
SplineCNN	99.22%	95.22%
geo-GCN	**99.36%**	**95.95%**

Incomplete image classification

Graph representation of images can be useful to describe images with missing regions. In this case, each visible pixel represents a node which is connected with its visible neighbors. Unobserved pixels are not represented in this graph.

For the evaluation, we considered MNIST dataset, where a square patch of the size 13x13 was removed from each image. The location of the patch was uniformly sampled for each image. For a comparison, we used imputation methods, which fill missing regions at preprocessing stage. Imputations were created using:

- *mean*: Missing features were replaced with mean values of those features computed for all (incomplete) training samples.

- *k-nn*: Missing attributes were filled with mean values of those features computed from the k nearest training samples (we used K = 5). Neighborhood was measured using Euclidean distance in the subspace of observed features.

- *mice*: This method fills absent pixels in an iterative process using Multiple Imputation by Chained Equation (mice), where several imputations are drawing from the conditional distribution of data by Markov chain Monte Carlo techniques

Completed MNIST images were processed by fully connected and convolutional neural networks. For complete MNIST images (no missing data), these networks obtained 98.79% and 99.34% of classification accuracy, respectively.

Table 2: Classification accuracy of graph representations of incomplete MNIST images.

Method	Accuracy
FCNet + mean	87.59%
FCNet + k-NN	87.10%
FCNet + mice	88.59%
ConvNet + mean	90.95%
ConvNet + k-NN	90.67%
ConvNet + mice	92.10%
geo-GCN	**92.40%**

The results presented in Table 2 show that geo-GCN gives better accuracy than all imputation methods on both versions of neural networks. The overall performance of geo-GCN is impressive, because geo-GCN does not use any ad-

ditional information concerning missing regions. This suggests that it is better to leave unobserved features missing than to complete them with inappropriate values, which is usually a common practice.

Learning from molecules

In the next experiment, we use chemical tasks to evaluate our model. We chose 3 datasets from MoleculeNet (Wu et al. 2018) which is a benchmark for molecule-related tasks. Blood-Brain Barrier Permeability (BBBP) is a binary classification task of predicting whether or not a given compound is able to pass through the barrier between blood and the brain, allowing the drug to impact the central nervous system. The ability of a molecule to penetrate this border depends on many different properties such as lipophilicity, molecule size, and its flexibility. Another 2 datasets, ESOL and FreeSolv, are solubility prediction tasks with continuous targets.
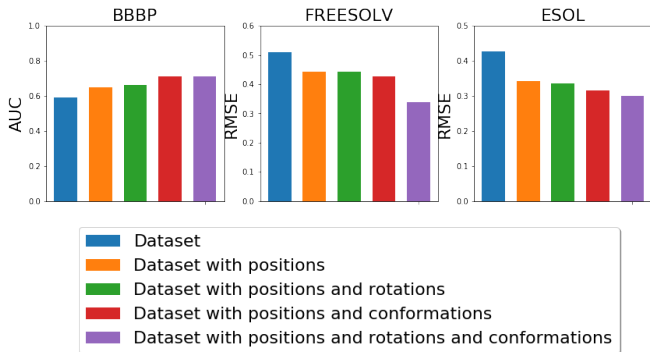

Figure 4: Comparison of different augmentation strategies on three chemical datasets. Dataset denotes a variant without information about positions (pure GCN). Positions were predicted with the UFF method. In the conformation variant multiple conformations were precalculated and then sampled during training. Rotation augmentation randomly rotates molecules in batches. For the first bar-plot higher is better, for the second and the third lower is better.

None of the three datasets contain atom positions, so only the graph representation of a compound can be obtained. However, the three-dimensional shape of a molecule can be predicted using energy minimization, which is fairly easy to do especially for small compounds. We run universal force field (UFF) method from RDKit package to predict atom positions. Because in our method we use absolute positions, and chemical compounds do not have one canonical orientation, the positional data can be augmented with random rotations. We also run UFF a few times (up to 30) to augment the data as this procedure is not deterministic.

To evaluate our model against methods proposed by MoleculeNet, we split the datasets into train, validation, and test subsets. The splits are done according to the MoleculeNet proposition that ESOL and FreeSolv datasets should be splitted at random, and BBBP data is splitted with a scaffold split that prevents similar structures to be put into differ-

ent sets – this way an algorithm cannot memorize the structures highly correlated with labels, but it needs to learn more general compound features. We run random search for all models testing 100 hyperparameter sets for each of them. All runs are repeated 3 times. The tuned hyperparameters of all tested methods are shown in the supplementary materials.

We benchmark our approach against popular chemistry models: graph-based models (Graph Convolution (Duvenaud et al. 2015), Weave Model (Kearnes et al. 2016), and Message Passing Neural Network (Gilmer et al. 2017)) as well as classical methods such as random forest and SVM, which often perform superbly in chemical tasks where datasets tend to be small (e.g. FreeSolv has only 513 compounds in its training set). Neither RF nor SVM operates on graphs, but rather they use calculated feature vectors which describe a molecule. In our comparison, ECFP (Rogers and Hahn 2010) was used for this purpose. In addition, EAGCN (Shang et al. 2018) is included in the experiment as the method that utilizes edge attributes together with the graph structure. As for our method, we show results with train- and test-time augmentation of the data carried out in the manner described above. For all datasets, we observe slight improvements with the augmented data. In order to investigate the impact of positional features, we also enrich the atom representation of the classical graph convolutional network with our predicted atom positions and apply the same procedure of augmentation. We name this enriched architecture pos-GCN and include it in the comparison.

Table 3: Performance on three chemical datasets measured with ROC AUC for BBBP and RMSE for ESOL and FreeSolv datasets. Best mean results and intervals overlapping with them are bolded. For the first column higher is better, for the second and the third lower is better.

Method	BBBP	ESOL	FreeSolv
SVM	0.603 ± 0.000	0.493 ± 0.000	0.391 ± 0.000
RF	0.551 ± 0.005	0.533 ± 0.003	0.550 ± 0.004
GC	0.690 ± 0.015	0.334 ± 0.017	$\mathbf{0.336 \pm 0.043}$
Weave	0.703 ± 0.012	0.389 ± 0.045	0.403 ± 0.035
MPNN	0.700 ± 0.019	0.303 ± 0.012	$\mathbf{0.299 \pm 0.038}$
EAGCN	0.664 ± 0.007	0.459 ± 0.019	0.410 ± 0.014
pos-GCN	0.696 ± 0.008	0.301 ± 0.011	$\mathbf{0.278 \pm 0.024}$
geo-GCN	$\mathbf{0.743 \pm 0.004}$	$\mathbf{0.270 \pm 0.005}$	$\mathbf{0.299 \pm 0.033}$

The results presented in Table 3 show that for FreeSolv dataset our method matches the result of MPNN, which is the best performing model for this task. For the two other datasets, geo-GCN outperforms all tested models by a significant margin. Based on pos-GCN scores, we notice that including positional features consistently improves the performance of the model across all tasks, and for the smallest dataset, FreeSolv, pos-GCN even surpasses the score of MPNN. Nevertheless, learning from bigger datasets requires a better way of managing positional data, which can be noted for ESOL and BBBP datasets for which pos-GCN performs significantly worse than geo-GCN but still better
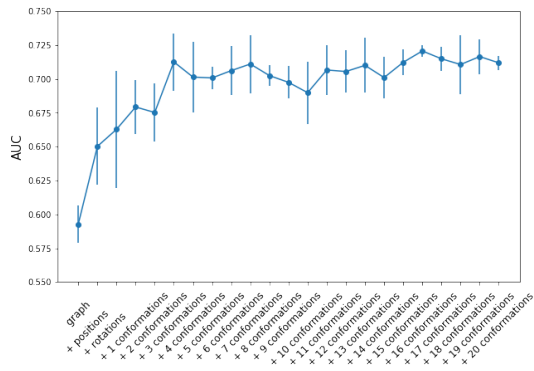
than vanilla GC.

Figure 5: ROC AUC scores measured on the BBBP dataset for different data augmentation strategies. The amount of augmentation increases from left to right.

Ablation study of the data augmentation

We also studied the effect of data augmentation on the geo-GCN performance. First, we examined how removing predicted positions, and thus setting all positional vectors to zero in Equation 3, affects the scores achieved by our model on chemical tasks. The results are depicted in Figure 4. It clearly shows that even predicted node coordinates improve the performance of the method. On the same plot we also show the outcome of augmenting the data with random rotations and 30 predicted molecule conformations, which were calculated as described in the previous subsection. As expected, the best performing model uses all types of position augmentation.

Eventually, the impact of various levels of augmentation was studied. For this purpose we precalculated 20 molecular conformations on the BBBP dataset using the universal force field method and used these predictions to augment the dataset. To test the importance of conformation variety, each run we increased the number of available conformations to sample from. The results are presented in Figure 5. One can see that including a bigger number of conformations helps the model to achieve better results. Also, the curve flattens out after a few conformations, which may be caused by limited flexibility of small compounds and high similarity of the predicted shapes.

Conclusion

We proposed geo-GCN which is a general model for processing graph-structured data with spatial features. Node positions are integrated into our convolution operation to create a layer which generalizes both GCNs and CNNs. In contrast to the majority of other approaches, our method can effectively use added information about location to construct self-taught feature masking, which can be augmented to achieve invariance of desired properties. Furthermore, we provide a theoretical analysis of our geometric graph convolutions. Experiments confirm strong performance of our method.

References

[Bruna et al. 2013] Bruna, J.; Zaremba, W.; Szlam, A.; and LeCun, Y. 2013. Spectral networks and locally connected networks on graphs. *arXiv preprint arXiv:1312.6203*.

[Cho, Choi, and others 2018] Cho, H.; Choi, I.; et al. 2018. Three-dimensionally embedded graph convolutional network (3dgcn) for molecule interpretation. *arXiv preprint arXiv:1811.09794*.

[Defferrard, Bresson, and Vandergheynst 2016] Defferrard, M.; Bresson, X.; and Vandergheynst, P. 2016. Convolutional neural networks on graphs with fast localized spectral filtering. In *Advances in neural information processing systems*, 3844–3852.

[Duvenaud et al. 2015] Duvenaud, D. K.; Maclaurin, D.; Iparraguirre, J.; Bombarell, R.; Hirzel, T.; Aspuru-Guzik, A.; and Adams, R. P. 2015. Convolutional networks on graphs for learning molecular fingerprints. In *Advances in neural information processing systems*, 2224–2232.

[Fey et al. 2018] Fey, M.; Eric Lenssen, J.; Weichert, F.; and Müller, H. 2018. Splinecnn: Fast geometric deep learning with continuous b-spline kernels. In *Proceedings of the IEEE Conference on Computer Vision and Pattern Recognition*, 869–877.

[Gilmer et al. 2017] Gilmer, J.; Schoenholz, S. S.; Riley, P. F.; Vinyals, O.; and Dahl, G. E. 2017. Neural message passing for quantum chemistry. In *Proceedings of the 34th International Conference on Machine Learning-Volume 70*, 1263–1272. JMLR. org.

[Gori, Monfardini, and Scarselli 2005] Gori, M.; Monfardini, G.; and Scarselli, F. 2005. A new model for learning in graph domains. In *Proceedings. 2005 IEEE International Joint Conference on Neural Networks, 2005.*, volume 2, 729–734. IEEE.

[Hamilton, Ying, and Leskovec 2017] Hamilton, W.; Ying, Z.; and Leskovec, J. 2017. Inductive representation learning on large graphs. In *Advances in Neural Information Processing Systems*, 1024–1034.

[Henaff, Bruna, and LeCun 2015] Henaff, M.; Bruna, J.; and LeCun, Y. 2015. Deep convolutional networks on graph-structured data. *arXiv preprint arXiv:1506.05163*.

[Kearnes et al. 2016] Kearnes, S.; McCloskey, K.; Berndl, M.; Pande, V.; and Riley, P. 2016. Molecular graph convolutions: moving beyond fingerprints. *Journal of computer-aided molecular design* 30(8):595–608.

[Kim 2014] Kim, Y. 2014. Convolutional neural networks for sentence classification. *arXiv preprint arXiv:1408.5882*.

[Kipf and Welling 2016] Kipf, T. N., and Welling, M. 2016. Semi-supervised classification with graph convolutional networks. *arXiv preprint arXiv:1609.02907*.

[Krizhevsky, Sutskever, and Hinton 2012] Krizhevsky, A.; Sutskever, I.; and Hinton, G. E. 2012. Imagenet classification with deep convolutional neural networks. In *Advances in neural information processing systems*, 1097–1105.

[Li et al. 2015] Li, Y.; Tarlow, D.; Brockschmidt, M.; and Zemel, R. 2015. Gated graph sequence neural networks. *arXiv preprint arXiv:1511.05493*.

[Li et al. 2018] Li, R.; Wang, S.; Zhu, F.; and Huang, J. 2018. Adaptive graph convolutional neural networks. In *Thirty-Second AAAI Conference on Artificial Intelligence*.

[Monti et al. 2017] Monti, F.; Boscaini, D.; Masci, J.; Rodola, E.; Svoboda, J.; and Bronstein, M. M. 2017. Geometric deep learning on graphs and manifolds using mixture model cnns. In *Proceedings of the IEEE Conference on Computer Vision and Pattern Recognition*, 5115–5124.

[Rogers and Hahn 2010] Rogers, D., and Hahn, M. 2010. Extended-connectivity fingerprints. *Journal of chemical information and modeling* 50(5):742–754.

[Scarselli et al. 2008] Scarselli, F.; Gori, M.; Tsoi, A. C.; Hagenbuchner, M.; and Monfardini, G. 2008. The graph neural network model. *IEEE Transactions on Neural Networks* 20(1):61–80.

[Seferbekov et al. 2018] Seferbekov, S. S.; Iglovikov, V.; Buslaev, A.; and Shvets, A. 2018. Feature pyramid network for multi-class land segmentation. In *CVPR Workshops*, 272–275.

[Shang et al. 2018] Shang, C.; Liu, Q.; Chen, K.-S.; Sun, J.; Lu, J.; Yi, J.; and Bi, J. 2018. Edge attention-based multi-relational graph convolutional networks. *arXiv preprint arXiv:1802.04944*.

[Veličković et al. 2017] Veličković, P.; Cucurull, G.; Casanova, A.; Romero, A.; Lio, P.; and Bengio, Y. 2017. Graph attention networks. *arXiv preprint arXiv:1710.10903*.

[Wu et al. 2018] Wu, Z.; Ramsundar, B.; Feinberg, E. N.; Gomes, J.; Geniesse, C.; Pappu, A. S.; Leswing, K.; and Pande, V. 2018. Moleculenet: a benchmark for molecular machine learning. *Chemical science* 9(2):513–530.

[Wu et al. 2019] Wu, F.; Zhang, T.; Souza Jr, A. H. d.; Fifty, C.; Yu, T.; and Weinberger, K. Q. 2019. Simplifying graph convolutional networks. *arXiv preprint arXiv:1902.07153*.

[Xu et al. 2018] Xu, K.; Hu, W.; Leskovec, J.; and Jegelka, S. 2018. How powerful are graph neural networks? *arXiv preprint arXiv:1810.00826*.

[Yang et al. 2015] Yang, J.; Nguyen, M. N.; San, P. P.; Li, X. L.; and Krishnaswamy, S. 2015. Deep convolutional neural networks on multichannel time series for human activity recognition. In *Twenty-Fourth International Joint Conference on Artificial Intelligence*.

[Yang et al. 2017] Yang, L.; Tang, K.; Yang, J.; and Li, L.-J. 2017. Dense captioning with joint inference and visual context. In *Proceedings of the IEEE Conference on Computer Vision and Pattern Recognition*, 2193–2202.

[Zhou and Li 2017] Zhou, Z., and Li, X. 2017. Convolution on graph: A high-order and adaptive approach. *arXiv preprint arXiv:1706.09916*.

Experimental details

In the following section we list out all hyperparameters ranges used during the random search in our experiments.

In table 4 we present the geo-GCN hyperparameters ranges, that were used in all our experiments.

Table 4: geo-GCN hyperparameter ranges

	parameters
batch size	16, 32, 64, 128
learning rate	0.01, 0.005, 0.001, 0.0005, 0.0001
model dropout	0.0, 0.1, 0.2, 0.3
layers number	1, 2, 4, 6, 8
model h dim	16, 32, 64, 128, 256, 512
model t dim	8, 16, 32, 64
use cluster pooling	True, False

Chemistry experiments

Below we list the hyperparameters ranges used in the chemistry experiment.

Table 5: SVM hyperparameter ranges

	parameters
C	0.25, 0.4375, 0.625, 0.8125, 1., 1.1875, 1.375, 1.5625, 1.75, 1.9375, 2.125, 2.3125, 2.5, 2.6875, 2.875, 3.0625, 3.25, 3.4375, 3.625, 3.8125, 4.
gamma	0.0125, 0.021875, 0.03125, 0.040625, 0.05, 0.059375, 0.06875, 0.078125, 0.0875, 0.096875, 0.10625, 0.115625, 0.125, 0.134375, 0.14375, 0.153125, 0.1625, 0.171875, 0.18125, 0.190625, 0.2

Table 6: RF hyperparameter ranges

	parameters
estimators number	125, 218, 312, 406, 500, 593, 687, 781, 875, 968, 1062, 1156, 1250, 1343, 1437, 1531, 1625, 1718, 1812, 1906, 2000

Table 7: GC hyperparameter ranges

	parameters
batch size	64, 128, 256
learning rate	0.002, 0.001, 0.0005
filters number	64, 128, 192, 256
fully connected nodes number	128, 256, 512

Table 8: Weave hyperparameter ranges

	parameters
batch size	16, 32, 64, 128
epochs number	20, 40, 60, 80, 100
learning rate	0.002, 0.001, 0.00075, 0.0005
graph features number	32, 64, 96, 128, 256
pair features number	14

Table 9: MPNN hyperparameter ranges

	parameters
batch size	8, 16, 32, 64
epochs number	25, 50, 75, 100
learning rate	0.002, 0.001, 0.00075, 0.0005
T	1, 2, 3, 4, 5
M	2, 3, 4, 5, 6

Table 10: EAGCN hyperparameter ranges

	parameters
batch size	16, 32, 64, 128, 256, 512
EAGCN structure	'concate', 'weighted'
epochs number	100, 500, 1000
learning rate	0.01, 0.005, 0.001, 0.0005, 0.0001
dropout	0.0, 0.1, 0.3
weight decay	0.0, 0.001, 0.01, 0.0001
sgc1 1	30, 60
sgc1 2	5, 10, 15, 20, 30
sgc1 3	5, 10, 15, 20, 30
sgc1 4	5, 10, 15, 20, 30
sgc1 5	5, 10, 15, 20, 30
sgc2 1	30, 60
sgc2 2	5, 10, 15, 20, 30
sgc2 3	5, 10, 15, 20, 30
sgc2 4	5, 10, 15, 20, 30
sgc2 5	5, 10, 15, 20, 30
den1	12, 32, 64
den2	12, 32, 64

Missing data experiments

Below we list the hyperparameters ranges used in the missing data experiment.

Table 11: Fully Connected Network hyperparameter ranges

	parameters
batch size	16, 32, 64, 128
learning rate	0.0001, 0.0005, 0.001, 0.005
layers dimensionality	64, 128, 256, 512
layers number	2, 3, 4, 5